RAPID COMMUNICATIONS

Temperature- and current-dependent spontaneous emission study on 2 μm InGaSb/AlGaAsSb quantum well lasers

Japanese Journal of Applied Physics **56**, 050310 (2017) **RAPID COMMUNICATION**
https://doi.org/10.7567/JJAP.56.050310

Temperature- and current-dependent spontaneous emission study on 2 μm InGaSb/AlGaAsSb quantum well lasers

Xiang Li[1], Hong Wang[1*], Zhongliang Qiao[1,4], Yongping Liao[2], Yu Zhang[2], Yingqiang Xu[2], Zhichuan Niu[2*], Cunzhu Tong[3], and Chongyang Liu[1]

[1]*School of Electrical and Electronic Engineering, Nanyang Technological University, 639798 Singapore*
[2]*State Key Lab for Superlattices and Microstructures, Institute of Semiconductors, Chinese Academy of Sciences, Beijing 100083, China*
[3]*State Key Lab of Luminescence and Applications, Changchun Institute of Optics, Fine Mechanics and Physics, Chinese Academy of Sciences, Changchun 130033, China*
[4]*The National Key Laboratory on High Power Semiconductor Lasers, Changchun University of Science and Technology, Changchun 130022, China*

*E-mail: ewanghong@ntu.edu.sg; zcniu@semi.ac.cn

Received December 22, 2016; accepted February 17, 2017; published online April 20, 2017

Spontaneous emission measurements, as a function of injection current and temperature, were carried out from the sidewall of a working 2 μm InGaSb/AlGaAsSb quantum well laser. The local Z power parameter was extracted to investigate the carrier recombination behaviors. A model involving the activation energy is presented to interpret the carrier loss mechanisms. Our findings show that the majority of the injected carriers recombine radiatively at low injection currents, and that Auger nonradiative recombination increases significantly with injection current. More importantly, no obvious temperature dependence of Z is observed from 20 to 80 °C. © 2017 The Japan Society of Applied Physics

Light sources operating in the 2 μm range are very promising for many applications such as gas sensing and advanced telecommunications.[1–3] High-performance 2 μm laser diodes have been demonstrated in both InP-based[4,5] and GaSb-based[6–9] quantum well (QW) laser structures. Compared with highly strained InGaAs QWs on InP substrates, GaSb-based QW lasers are less challenging in material growth and thus more advantageous when it comes to some longer wavelength applications. Researchers have achieved ultralow-threshold current density (J_{th}),[6] high power,[7] low lateral divergence,[8] and high-performance vertical-cavity surface-emitting lasers[9] in GaSb-based laser systems in the 2 μm range. Despite these numerous achievements, fundamental investigations are still highly desirable to understand the ultimate limits of the devices.[10] For instance, the carrier recombination behaviors and loss mechanisms within QWs directly affect the laser performance characteristics such as temperature characteristics, J_{th}, and so on. In addition, there is an intrinsic drawback in GaSb-based QW light-emitting devices, which is the inadequate confinement of holes in the active region, and the impacts of this drawback on the carrier recombination behaviors have not been revealed experimentally. Therefore, a systematic investigation of the carrier recombination behaviors will be useful for further optimizing GaSb-based QW lasers.

Since spontaneous emission (SE) reflects directly the intensity of carrier recombination below the lasing threshold, the measurement of SE has been used as a powerful tool to investigate the intrinsic recombination mechanisms in several electrical injection lasers such as GaAs-based QW, quantum dot (QD), submonolayer QD, and InP-based QW lasers.[11–16] However, a systematic SE study of the effects of both injection current (I_{bias}) and working temperature (T) in GaSb-based lasers remains lacking.

In this work, temperature-dependent SEs at different biasing currents have been measured using a working 2 μm InGaSb/AlGaAsSb QW laser. By extracting and analyzing the local Z power parameter, better insights into the effects of I_{bias} and T on the carrier recombination mechanisms are obtained. In addition, the carrier loss mechanisms have also been investigated in detail.

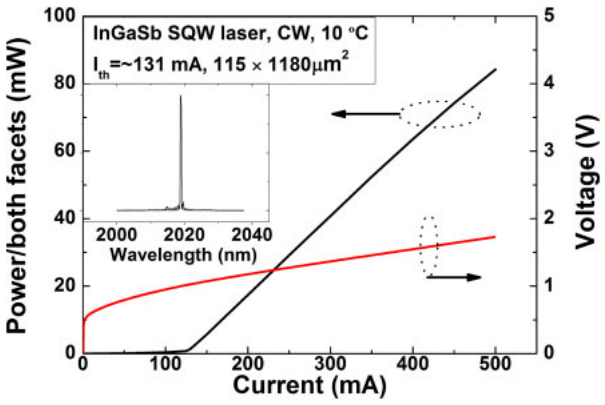

Fig. 1. (Color online) L–I–V curve of the fabricated InGaSb SQW laser at 10 °C. The inset shows its lasing spectrum.

The laser used in this study comprises an $In_{0.2}Ga_{0.8}Sb$ single QW (SQW) with a lattice-matched $Al_{0.2}GaAs_{0.02}Sb$ barrier grown on a GaSb substrate by molecular beam epitaxy (MBE). The detailed laser structure can be found in our previous work.[1] A typical wet ridge etching and contact window opening process[17] was used to fabricate Fabry–Perot (FP) ridge waveguide lasers with different ridge widths on the same wafer. The cleaved single laser chip was bonded p-side down on a heatsink to facilitate heat dissipation. A temperature electronic controller (TEC) was used for temperature control during the measurements.

Figure 1 shows the light output power and voltage as a function of the injection current (L–I–V) for one of the fabricated lasers. The InGaSb SQW laser works well in the continuous wave (CW) mode at 10 °C with a low J_{th} of ~96 A/cm^2, which suggests good material quality. The lasing spectrum centering at ~2019 nm is also shown in the inset of Fig. 1.

The SE was measured from the sidewall of the laser as schematically shown in the inset of Fig. 2. It was collected by a multimode optical fiber and fed into an optical spectrum analyzer (OSA; AQ6375). Since there is almost no feedback in the direction perpendicular to the laser ridge, the measured

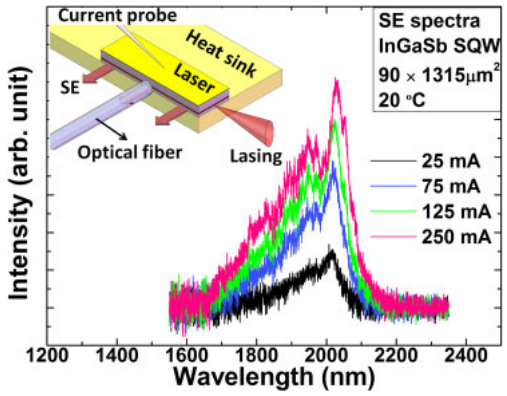

Fig. 2. (Color online) SE spectra of the tested laser at four different I_{bias} values at 20 °C. The inset shows the schematic diagram of the SE measurement configuration (not to scale).

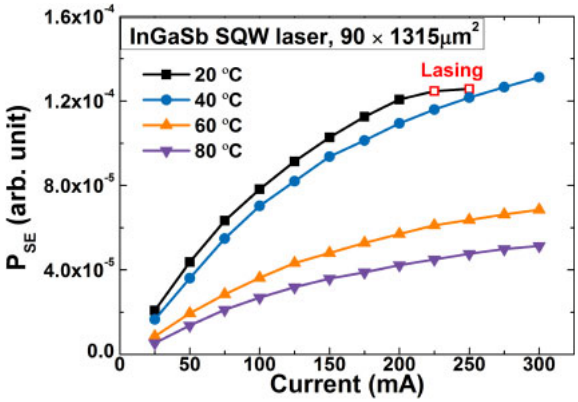

Fig. 3. (Color online) Integrated SE intensities (P_{SE}) at different I_{bias} values calculated from the SE spectra at four different temperatures (20, 40, 60, and 80 °C). The hollow squares represent the results obtained after lasing at 20 °C.

SE does not undergo significant amplification or absorption.[11,12] The laser used for SE measurements is from the same fabrication batch as the laser in Fig. 1. Prior to SE measurements, the CW operation of the laser was measured at 20 °C. Then, SE spectra were recorded at different I_{bias} values from 25 mA with a step of 25 mA. For clarity, SE spectra at four different I_{bias} values measured at 20 °C are shown in Fig. 2. The SE spectral intensity increases with I_{bias} and the spectral peaks locate at ~2020 nm, which is almost identical to that of the lasing spectrum. This peak is attributed to the transition from the first electron band (E1) to the first heavy-hole band (HH1) on the basis of band structure calculations.[1)]

The integrated SE intensities (P_{SE}) at different I_{bias} values at 20 °C were calculated from the SE spectra as shown in Fig. 3 (squares). It is well known that P_{SE} can reflect the carrier density (n) within QWs, and theoretically, when the lasing action starts, n will be pinned at its threshold owing to the intense stimulated recombination. Therefore, P_{SE} should also be pinned at the lasing threshold. This postulation is confirmed by the experimental data at 20 °C in Fig. 3: P_{SE} remains almost unchanged after lasing (shown by hollow squares). The same phenomenon has also been observed in our GaAs-based QD laser[11)] and some InP-based QW lasers.[18)]

To analyze the carrier recombination behaviors with the variation in I_{bias}, the following model,[11,19)] which gives the relationship between I_{bias} and P_{SE}, was used:

$$I_{bias} = \left(\frac{e^2V}{R}\right)^{1/2}\left(\frac{1}{\tau_{nr}^2 B}\right)\left(\sqrt{P_{SE}}\right)^1 + \frac{e}{R}\left(\sqrt{P_{SE}}\right)^2 + \left(\frac{e^2}{R^3V}\right)^{1/2}\left(\frac{C}{B^{3/2}}\right)\left(\sqrt{P_{SE}}\right)^3, \quad (1)$$

where e is the electron charge, V is the volume of the active region, R is the ratio of the detected intensity P_{SE} to the actual intensity P (i.e., $P_{SE} = R \times P$), τ_{nr} is the nonradiative lifetime, and B and C are the radiative recombination and Auger recombination coefficients, respectively.

In this model, prior to lasing, the injected carriers are supposed to have the following three recombination processes that correspond to the three terms on the right-hand side of Eq. (1):

1) defect- or impurity-related nonradiative recombination (NR) whose rate is proportional to the carrier density n in the active region and which can be written as $R_d = V(n/\tau_{nr})$;[19)]
2) radiative recombination whose rate is proportional to n^2 and which can be written as $R_{spon} = VBn^2$;[19)] and
3) Auger NR whose rate is proportional to n^3 and which can be expressed as $R_A = VCn^3$.[19)]

The three terms on the right-hand side of Eq. (1) have the factor $\left(\sqrt{P_{SE}}\right)$, so Eq. (1) can be expressed as

$$I_{bias} \propto \left(\sqrt{P_{SE}}\right)^Z, \quad (2)$$

where Z is the local Z power parameter, which ranges from 1 to 3 if the current is dominated by defect- or impurity-related NR ($Z \approx 1$), radiative recombination ($Z \approx 2$), or Auger NR ($Z \approx 3$). The actual Z value reflects the proportions of these three recombination processes. Note that this model does not consider the carrier leakage that may cause Z to be more than 3. Furthermore, in view of the extremely low J_{th} of our InGaSb laser, the material is believed to be of high quality and the defect-related NR process would be weak and ignorable.

To extract the Z values of the tested laser at 20 °C, $\ln I_{bias}$ is plotted against $\ln P_{SE}^{1/2}$ in Fig. 4(a) (squares indicate the experimental data). The Z values are the slopes of this plot and can be obtained by second-order polynomial fitting to the experimental data shown by dashed lines in the figure. The Z values at 20 °C are shown in Fig. 4(b) (squares). Z increases with I_{bias}, which is due to the following reasons: when I_{bias} increases, n within the active region also increases. Since the rate of Auger NR follows n^3, while it is on the order of n^2 for radiative recombination, the contribution of Auger NR will increase. This in-turn increases the Z value from 2 to 3. Note that the Z value exceeds 3 when $I_{bias} = 150$ mA, suggesting that carrier leakage (thermionic carrier emission to the outside of the QW) cannot be ignored at high I_{bias} values.[11)]

Subsequently, in order to investigate how working temperature affects the carrier recombination behaviors, the SE spectra at 40, 60, and 80 °C were measured. Figure 3 shows the calculated P_{SE} values at such temperatures, and the double logarithmic plots at these three temperatures are shown in Fig. 4(a). As can be seen from the figure, the four

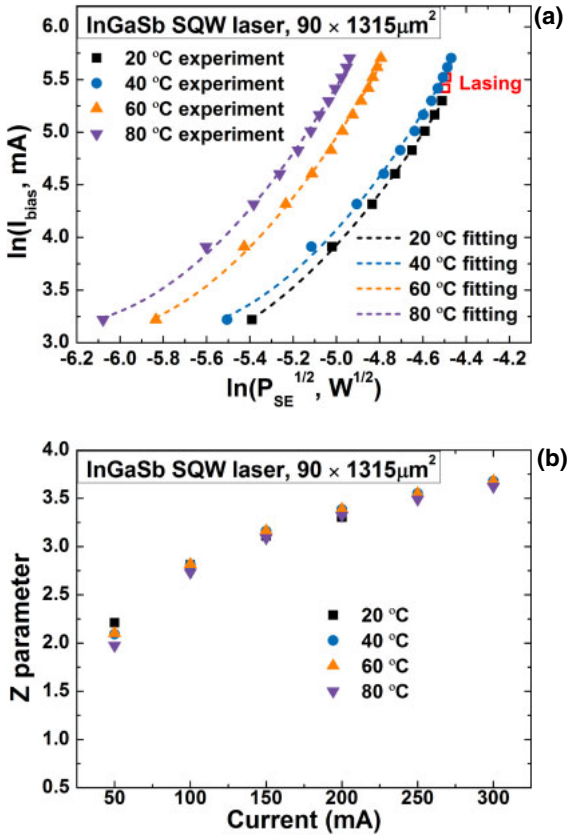

Fig. 4. (Color online) (a) Double logarithmic plots of $\ln I_{\mathrm{bias}}$ as a function of $\ln P_{\mathrm{SE}}^{1/2}$ at four different temperatures (20, 40, 60, and 80 °C). The points are the experimental data, while the dashed lines show the second-order polynomial fitting curves of the experimental data. (b) Z values as a function of I_{bias} at above four temperatures.

fitting curves are almost parallel to each other, indicating that there is no distinct difference between the Z values at different temperatures. This can be seen more clearly in Fig. 4(b), in which Z is I_{bias}-dependent rather than T-dependent.

The Z value is around 2 at a low I_{bias} (50 mA), suggesting that the majority of the injected carriers recombine radiatively, and the laser exhibits a very high efficiency under low injection currents. Increasing Z to around 3.1 when I_{bias} is 150 mA indicates that Auger NR becomes dominant at high current injection. With further increase in I_{bias}, the lasing action initiates in the 20 °C case and Z becomes almost infinite. In the higher temperature cases, a Z value as high as 3.6 at 300 mA is observed. Such a high Z value could be attributed to the increased carrier leakage at high I_{bias} values.

The Z value is insensitive to temperature, which is a consequence of the power law dependences of the recombination processes on the carrier density n included in the applied model. First, it is commonly observed that, under the same I_{bias}, n decreases with working temperature owing to a more severe carrier loss, which causes a larger Z value. Moreover, the radiative recombination rate R_{spon} is proportional to n^2, while the Auger NR rate R_{A} is proportional to n^3. R_{A} decreases more significantly when temperature increases, which results in a smaller Z value. Under the effects of these two mechanisms, Z maintains a fixed value. This finding

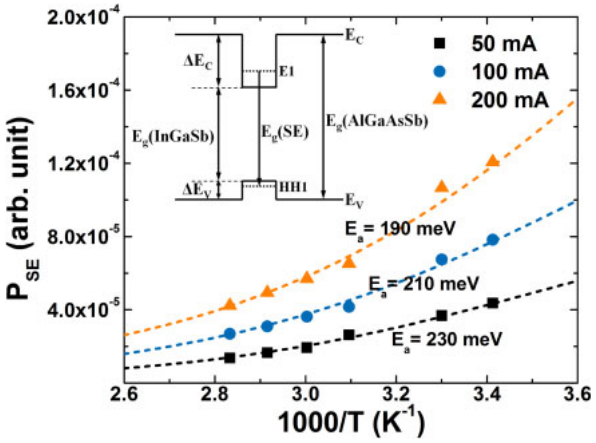

Fig. 5. (Color online) Arrhenius plot of P_{SE} at three different I_{bias} values (50, 100, and 200 mA). The points are the experimental data, while the dashed lines show the fitting curves of the experimental data obtained using a model that involves the activation energy. The inset shows the band structure of the QW and barrier.

also implies that, at higher temperatures, thermionic carrier emission may replace Auger NR to become the dominant NR process. A similar phenomenon has also been found in 1.55 μm InP QW lasers.[20)]

To further investigate the carrier loss mechanisms with respect to I_{bias} and T, P_{SE} is plotted as a function of $1000/T$ at three different I_{bias} values (50, 100, and 200 mA) as shown in Fig. 5. The temperature-dependent SE follows the Arrhenius dependence and can be interpreted using the model below, and the activation energy (E_{a}) can be extracted by it.

$$P_{\mathrm{SE}}(T) = \frac{I_0}{1 + C_{\mathrm{NR}} \exp(-E_{\mathrm{a}}/k_{\mathrm{B}}T)}, \tag{3}$$

where I_0 and C_{NR} are constants, E_{a} is the activation energy, and k_{B} is the Boltzmann constant. The best fit to the experiment data gives E_{a} values of 230, 210, and 190 meV at 50, 100, and 200 mA, respectively.

It is believed that E_{a} is related to the total confinement energy (E_{Total}) of carriers in the QW region.[21)] E_{Total} of an electron–hole pair in a QW can be expressed as E_{g}(Barrier) − E_{g}(SE), as shown in the inset of Fig. 5. In our laser structure, the barrier material is lattice-matched $Al_{0.2}GaAs_{0.02}Sb$ whose band gap is determined to be ∼964 meV using the equation given by Vurgaftman et al.[22)] In the 20 °C case, the SE peaks locate at ∼2020 nm [E_{g}(SE) ≃ 614 meV]. These results correspond to an E_{Total} of ∼350 meV. The valence band offsets (VBOs) of the $Al_{0.2}GaAs_{0.02}Sb$ barrier and $In_{0.2}Ga_{0.8}Sb$ QW are calculated by linear interpolations using Eq. (4) and the band parameters are also given by Vurgaftman et al.[22)] In addition, since $In_{0.2}Ga_{0.8}Sb/Al_{0.2}GaAs_{0.02}Sb$ has a compressive strain of ∼1.26%, the valence band of the QW will be shifted upward ∼13 meV on the basis of the model-solid theory.[18)] All these factors result in a final ΔE_{V} of ∼109.5 meV. Then, the energy from the top of the valence band to the first heavy-hole band is determined to be ∼7.5 meV by solving the one-dimensional (1D) finite potential well Schrödinger equation. Thus, the potential barrier heights of holes and electrons are ∼102 and ∼248 meV, respectively, in our designed $In_{0.2}Ga_{0.8}Sb/Al_{0.2}GaAs_{0.02}Sb$ QW structure.

$$\mathrm{VBO}_{\mathrm{Al}_x\mathrm{GaAs}_y\mathrm{Sb}} = \frac{x(1-x)[(1-y)\mathrm{VBO}_{\mathrm{Al}_x\mathrm{GaSb}} + y\mathrm{VBO}_{\mathrm{Al}_x\mathrm{GaAs}}] + y(1-y)[x\mathrm{VBO}_{\mathrm{AlAs}_y\mathrm{Sb}} + (1-x)\mathrm{VBO}_{\mathrm{GaAs}_y\mathrm{Sb}}]}{x(1-x) + y(1-y)}, \quad (4a)$$

The VBO of the ternary materials can be determined using the following equations:

$$\mathrm{VBO}_{\mathrm{A}_x\mathrm{B}_{1-x}\mathrm{C}} = x\mathrm{VBO}_{\mathrm{AC}} + (1-x)\mathrm{VBO}_{\mathrm{BC}} - x(1-x)C_{\mathrm{A}_x\mathrm{B}_{1-x}\mathrm{C}}, \quad (4b)$$

$$\mathrm{VBO}_{\mathrm{AB}_y\mathrm{C}_{1-y}} = y\mathrm{VBO}_{\mathrm{AB}} + (1-y)\mathrm{VBO}_{\mathrm{AC}} - y(1-y)C_{\mathrm{AB}_y\mathrm{C}_{1-y}}, \quad (4c)$$

where C is the bowing parameter.

By comparing the two barrier heights with E_a at the three different I_{bias} values, it can be found that, under a low I_{bias} (e.g., 50 mA), E_a fits the potential barrier height of electrons well. This indicates that, although the electron loss and the hole loss coexist throughout the entire current range for determining the overall E_a, the thermal loss of electrons is the dominant carrier loss mechanism under a low I_{bias}. The hole loss becomes more crucial, which is evident by the marked reduction in E_a towards the potential barrier height of holes, when I_{bias} increases. This reflects one intrinsic drawback in GaSb-based QW lasers, which is the poor confinement of holes in the active region. The results experimentally confirm the negative effects of this drawback and reveal its impacts on the carrier recombination behaviors. The total carrier loss increases owing to the decrease in E_a.

As determined from the results of the above analyses, the majority of the injected carriers recombine radiatively when I_{bias} is relatively low (e.g., 50 mA). With the increase in I_{bias}, Auger recombination becomes more significant and, at the same time, carrier leakage becomes evident. When the lasing action initiates, all the extra injected carriers beyond the threshold are consumed by stimulated emission only. Furthermore, there is no obvious temperature dependence of Z from 20 to 80 °C, which indicates that the contributions of the two NR processes (Auger NR and thermionic carrier emission) change as the working temperature increases, and thermionic carrier emission may overtake Auger NR as the dominant NR process at higher temperatures. These findings explain the power law dependences of the recombination processes on the carrier density included in the applied model. Also, as to the temperature characteristics of the laser, the severe thermal loss of holes at high I_{bias} cannot be ignored.

In conclusion, high-performance 2 μm InGaSb SQW lasers with the state-of-the-art low J_{th} of ~96 A/cm^2 are presented. The carrier recombination behaviors of the fabricated lasers are experimentally studied through SE measurements. By analyzing the calculated Z values, the evolutions of the carrier recombination behaviors along with the injection current and operating temperature are obtained. The effects of the inadequate confinement of holes on the carrier recombination behaviors are revealed. The findings provide guidelines for further improvement of GaSb-based lasers such as increasing ΔE_V through introducing more strain into QWs to provide better carrier confinement,[6] or applying quinary material barriers (AlGaInAsSb),[23] which may enhance the hole confinement, thus reducing J_{th} and enabling the lasers to work at higher temperatures.

Acknowledgments This work was supported in part by the National Research Foundation of Singapore (NRF-CRP12-2013-04), National Natural Science Foundation of China (61435012, 61308051), and National Key Basic Research Program of China (2014CB643903, 2013CB932904).

1) X. Li, H. Wang, Z. Qiao, Y. Zhang, Z. Niu, C. Tong, and C. Liu, IEEE J. Sel. Top. Quantum Electron. **22**, 1500507 (2016).
2) J. J. Ackert, D. J. Thomson, L. Shen, A. C. Peacock, P. E. Jessop, G. T. Reed, G. Z. Mashanovich, and A. P. Knights, Nat. Photonics **9**, 393 (2015).
3) G. Roelkens, U. Dave, A. Gassenq, N. Hattasan, C. Hu, B. Kuyken, F. Leo, A. Malik, M. Muneeb, and E. Ryckeboer, IEEE J. Sel. Top. Quantum Electron. **20**, 394 (2014).
4) W. Lei and C. Jagadish, J. Appl. Phys. **104**, 091101 (2008).
5) S. Luo, H. M. Ji, F. Gao, F. Xu, X. G. Yang, P. Liang, and T. Yang, Opt. Express **23**, 8383 (2015).
6) G. W. Turner, H. K. Choi, and M. J. Manfra, Appl. Phys. Lett. **72**, 876 (1998).
7) L. Shterengas, G. Belenky, M. V. Kisin, and D. Donetsky, Appl. Phys. Lett. **90**, 011119 (2007).
8) J. Rong, E. Xing, Y. Zhang, L. Wang, S. Shu, S. Tian, C. Tong, X. Chai, Y. Xu, H. Ni, Z. Niu, and L. Wang, Opt. Express **24**, 7246 (2016).
9) A. B. Ikyo, I. P. Marko, K. Hild, A. R. Adams, S. Arafin, M. C. Amann, and S. J. Sweeney, Sci. Rep. **6**, 19595 (2016).
10) X. Gao, Z. Wei, F. Zhao, Y. Yang, R. Chen, X. Fang, J. Tang, D. Fang, D. Wang, R. Li, X. Ge, X. Ma, and X. Wang, Sci. Rep. **6**, 29112 (2016).
11) C. Y. Liu, M. Stubenrauch, and D. Bimberg, Nanotechnology **22**, 235202 (2011).
12) K. Sears, M. Buda, H. H. Tan, and C. Jagadish, J. Appl. Phys. **101**, 013112 (2007).
13) S. L. Chuang, C. S. Chang, J. Minch, and W. Fang, Proc. SPIE **2994**, 522 (1997).
14) R. Fehse, S. Tomic, A. R. Adams, S. J. Sweeney, E. P. O'Reilly, A. Andreev, and H. Riechert, IEEE J. Sel. Top. Quantum Electron. **8**, 801 (2002).
15) L. L. Goddard, S. R. Bank, M. A. Wistey, H. B. Yuen, Z. Rao, and J. S. Harris, Jr., J. Appl. Phys. **97**, 083101 (2005).
16) D. Arsenijevic, C. Liu, A. Payusov, M. Stubenrauch, and D. Bimberg, IEEE Photonics Technol. Lett. **24**, 906 (2012).
17) C. Liu, H. Wang, Q. Meng, B. Gao, and K. S. Ang, Appl. Phys. Express **6**, 102702 (2013).
18) S. L. Chuang, *Physics of Optoelectronic Devices* (Wiley, New York, 1995) 1st ed., p. 409.
19) I. I. Novikov, N. Yu Gordeev, M. V. Maximov, Yu. M. Shernyakov, A. E. Zhukov, A. P. Vasil'ev, E. S. Semenova, V. M. Ustinov, N. N. Ledentsov, D. Bimberg, N. D. Zakharov, and P. Werner, Semicond. Sci. Technol. **20**, 33 (2005).
20) J. Piprek, P. Abraham, and J. E. Bowers, IEEE J. Quantum Electron. **36**, 366 (2000).
21) C. Liu, S. F. Yoon, J. Teng, J. Dong, and S. J. Chua, Appl. Phys. A **91**, 435 (2008).
22) I. Vurgaftman, J. R. Meyer, and L. R. Ram-Mohan, J. Appl. Phys. **89**, 5815 (2001).
23) G. Sęk, M. Motyka, F. Janiak, K. Ryczko, J. Misiewicz, A. Bauer, M. Dallner, R. Weih, S. Höfling, A. Forchel, S. Belahsene, G. Boissier, and Y. Rouillard, Proc. SPIE **8631**, 86312O (2013).